Effect of Organoclay on the Morphology and Properties of Poly(propylene)/Poly[(butylene succinate)-*co*-adipate] Blends

Suprakas Sinha Ray,* Jayita Bandyopadhyay, Mosto Bousmina

The effect of organically modified clay on the morphology and properties of poly(propylene) (PP) and poly[(butylene succinate)-*co*-adipate] (PBSA) blends is studied. Virgin and organoclay modified blends were prepared by melt-mixing of PP, PBSA and organoclay in a batch-mixer at 190 °C. Scanning electron microscopy studies revealed a significant change in morphology of PP/PBSA blend in the presence of organoclay. The state of dispersion of silicate layers in the blend matrix was characterized by X-ray diffraction and transmission electron microscopic observations. Dynamic mechanical analysis showed substantial improvement in flexural storage modulus of organoclay-modified blends with respect to the neat polymer matrices or unmodified blends. Tensile properties of virgin blends also improved in the presence of organoclay. Thermal stability of virgin blends in air atmosphere dramatically improved after modification with organoclay. The effect of organoclay on the melt-state liner viscoelastic properties of virgin blends was also studied. The non-isothermal crystallization behavior of homopolymers, virgin, and organoclay-modified blends were studied by differential scanning calorimeter. The effect of incorporation of organoclay on the cold crystallization behavior of PP/PBSA blends is also reported.

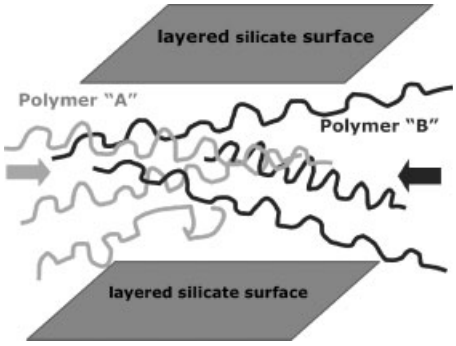

Introduction

In the last two decades of the 20th century one of the rapidly growing areas for the use of plastics was packaging. Convenience and safety, low price and good aesthetic qualities are the most important factors determining rapid growth in the use of plastics for manufacturing of packing. Recently, out of the total plastic production, 41% is used in the packing industry of which 47% is used for the packing of foodstuffs.[1,2] Due to its good cost to properties ratio as well as versatility, the material most often used is poly(propylene) (PP). PP is a thermoplastic polyolefin, is mostly produced from fossil fuels, consumed and discarded into the environment, ending up as spontaneously undegradable wastes. PP generally degrades in the presence of oxygen and ultraviolet rays;[3,4] however, the degradation process is extremely slow. To date, various approaches have been considered to render

S. Sinha Ray
National Centre for Nano-Structured Materials (NCNSM), Council for Scientific and Industrial Research, 1-Meiring Naude Road, Brummeria, PO Box 395, Pretoria 0001, Republic of South Africa
Fax: +27 12 841 2135; E-mail: RSuprakas@csir.co.za
J. Bandyopadhyay, M. Bousmina
Department of Chemical Engineering, Laval University, Sainte-Foy, Quebec G1K 7P4, Canada
E-mail: bousmina@gch.ulaval.ca

DOI: 10.1002/mame.200700029

PP degradable.[4] One of the most commonly used methods is to make blends of PP with a highly abundant and inexpensive naturally degradable polymer matrix.

In this respect, poly[(butylene succinate)-*co*-adipate] (PBSA) is among the most promising polymers. PBSA is a copolymer of poly(butylene succinate) (PBS) and shows a variety of interesting physical properties including biodegradability.[5] It is synthesized by the polycondensation of butane-1,4-diol in the presence of succinic and adipic acids with a relatively low production cost and satisfactory mechanical properties equivalent to that of PP.[5] The molecular structure of PBSA is presented in Figure 1. PBSA, compared with PBS, is more susceptible to biodegradation because of its lower crystallinity and more flexible polymer chains.[6] With its excellent processability, it is well suited to the field of textiles into melt blow, multifilament, monofilament, flat, and split yarn, and also in the field of plastics into injection molded products. It is thus a promising polymer for various applications.

However, most chemically different polymers are immiscible and their blending leads to materials with weak interfacial adhesion and thus poor mechanical performances. The conversion of the immiscible blend to a useful polymeric product with the desired properties requires some manipulations of the interface. One of the classical routes to ensure adhesion between the phases is the use of a third component, a compatibilizer, which is miscible or at least compatible with both phases.[7] Such a compatibilizer may be a homopolymer,[8,9] or a block, graft or star copolymer.[10–17] Incorporation of the compatibilizer into the blend matrix can be done either by addition[8] or by in situ generation in a reactive compatibilization process.[9,18] The compatibilization engenders the desired blend morphology by controlling the interfacial properties and thus the size of the dispersed droplets of the minor phase, it stabilizes the morphology against coalescence during the subsequent processing steps and furthermore ensures adhesion between the phases in the solid state, thus improving the mechanical properties. The result is a blend with a finer and more stable morphology along with enhanced interfacial performance. These 'classical' compatibilization strategies have been widely used to generate a variety of industrial polymer blends with a wide range of properties.[19]

Another recently explored compatibilization method for the immiscible polymer blend is that of the use of inorganic solid particles. In 1994, Tanaka et al.[20] first reported that the structural evolution of immiscible

$$[\text{-O-}\{(\text{CH2})_4\text{-O}\}_1\text{-}\{\text{CO-}(\text{CH}_2)_2\text{-CO-}\}_x\text{-}\{\text{CO-}(\text{CH}_2)_4\text{-CO-}\}_y\text{-}]$$

$$x+y = 1$$

Figure 1. Molecular structure of poly[(butylene succinate)-*co*-adipate] (PBSA).

polymer blends is affected by mobile glass particles, which inhibit the coarsening process by pinning one or more of the phases. Later, Ginzburg et al.[21] simulated the effect of motion of hard particles on the phase separation behavior of binary mixtures. According to them, the preferential wetting between the particles and one of the phases impedes the growth of the domains. They postulated that the mechanism for the slowing down of domain growth is due to the pinning effect of localized particles. Recently, Lipatov et al.[22–25] have shown that the incorporation of fumed silica into an immiscible polymer mixture may increase the compatibility between the two polymer matrices. They noted that in three components system of S (inorganic solid particles) with polymers A and B, the free energy of mixing (per unit volume) is given by:

$$\Delta G_m = \Delta G_{AS} + \Delta G_{BS} - \Delta G_{AB} \quad (1)$$

where the subscripts identify the interacting pairs. Thermodynamically the system is stable (i.e., $\Delta G_m < 0$) when the blend is immiscible with a positive value of ΔG_{AB} than miscible with negative value of ΔG_{AB} (i.e., $\Delta G_{AB} > 0$ and ΔG_{AS}, $\Delta G_{BS} < 0$). Thus, addition of S to A–B blend stabilizes it, that is, it acts as a compatibilizer by adsorbing A and/or B polymers on its surface. Evidently, the stabilizing energy gain originates from the adsorption of polymeric components on the solid surface. To play this role the inorganic phase should have the largest possible surface area per unit weight and be able to be dispersed well within the two-phase matrix. This requirement is nicely satisfied with clay such as montmorillonite (MMT) because it has the specific surface area of about $S_0 = 700–800\ m^2 \cdot g^{-1}$ and polymer chains can be intercalated into two dimensional silicate galleries.[26] Furthermore, clay platelets can bend, which provides an additional parameter that affects the domain size of the dispersed phase.

In recent years, several research groups have reported that organically modified clay can act as a compatibilizer for several types of immiscible polymer blends by effectively reducing the domain size of the dispersed particles.[27–50] Most authors attribute this effect to the clay acting as a physical barrier, which slows down coalescence of the dispersed phases by increasing the viscosity.[29,51] In this article we present experimental results of the incorporation of high aspect ratio organically modified montmorillonite (OMMT) in immiscible poly(propylene) (PP)/poly[(butylene succinate)-*co*-adipate] (PBSA) blends. First, the PP/PBSA blend was studied where intercalated layered silicate particles were preferentially located in the PBSA phase. Second, the PP grafted with maleic anhydride (PP-*g*-MA)/PBSA blends were studied where silicates layers were intercalated by both PP-*g*-MA and PBSA polymer chains. The effect of the concentration

Macromol. Mater. Eng. **2007**, *292*, 729–747

Macromolecular Journals

DOI: 10.1002/mame.200700029

of maleic anhydride grafting on blend morphology was also studied. The weight ratio of PP or PP-*g*-MA and PBSA is 80/20 and the OMMT concentration was fixed to 5 wt.-% to potentially minimize the effect of viscosity ratio on particles size. The morphology and properties of virgin and OMMT-modified blends were extensively investigated by scanning electron microscopy (SEM), X-ray diffraction (XRD) analysis, transmission electron microscopy (TEM), differential scanning calorimetry (DSC), dynamic mechanical analysis (DMA), mechanical testing in traction mode and thermogravimetric analysis (TGA). The melt rheological behaviors of unmodified and OMMT-modified blends are also described. On the basis of these results, a general understanding is described and an explanation given as to how organoclay platelets affect the morphology and properties of immiscible polymer blends.

Experimental Part

Materials

Clays are naturally hydrophilic, with cations loosely bonded between the sheets of oxygen and silicon.[26] Such layered silicates are about 1 nm thick but they have a large active surface area (700–800 $m^2 \cdot g^{-1}$) and a moderate surface charge. In their pristine form, they are not compatible with most of the polymeric materials. Therefore, the clay must be treated before its incorporation into the polymeric matrix. Organically modified clays are generally made by a cation exchange reaction between the intergalleries cations (generally Na^+ or K^+) cations and an alkylammonium or phosphonium salt. Alkylammonium or alkylphosphonium cations in the organosilicates lower the surface energy of the inorganic host and improve the wetting characteristics of the polymer matrix, and result in a larger interlayer spacing.

The organically modified clay used in this study was Cloisite® 20A (commercially abbreviated as C20A), supplied by the Southern Clay Products. According to the supplier the original clay was Na^+–MMT and intercalated with 38 wt.-% of *N,N*-dimethyl dihydrogenated tallow ammonium chloride (2M2ODA) salt.[52] Tallow is a mixture of octadecyl, hexadecyl, and tetradecyl with octadecyl being the major component (>60%).[29]

The PBSA used in this study was a commercial product from Showa High Polymer Ltd., Japan, with the designation BIONOLLE # 3001 ($\overline{M}_w = 190\ kg \cdot mol^{-1}$). The PP matrix used was a homopolymer Pro-fax PDC 1274 ($\overline{M}_w = 250\ kg \cdot mol^{-1}$). Two types of PP-*g*-MA were used in this study: Polybond® 3200 ($\overline{M}_w = 335\ kg \cdot mol^{-1}$, MA content 0.2 wt.-%) and Polybond® 3150 ($\overline{M}_w = 330\ kg \cdot mol^{-1}$, MA content: 0.5 wt.-%) from Crompton Co. The neat PP, PP with 0.2 wt.-% MA grafting, and PP with 0.5 wt.-% of MA grafting are correspondingly abbreviated as PPa, PPb, and PPc. All polymers were dried under vacuum at 75 °C for 36 h prior to use.

Blending

Blends of PP or PP-*g*-MA and PBSA with one weight composition were prepared under the same condition by first melting the polymers and then mixing of C20A for 10 min in Thermohaake twin-rotors mixer (Polylab system) at 190 °C (set temperature), and a rotor speed of 60 rpm. The blends were then compression molded using a Carver laboratory press at 190 °C for 10 min into sheets of 1.5 mm thick and then cooled at room temperature. The thermochemical history of all samples was identical. The weight ratio of PP or PP-*g*-MA and PBSA was 80/20. The C20A concentration was 5 wt.-% for each 80/20 PP/PBSA or PP-*g*-MA/PBSA weight ratio.

Characterization

The morphology of unmodified and C20A modified blends was investigated by means of SEM. The compression molded samples were kept in liquid nitrogen for 3 h and brittle fractured in liquid nitrogen. The fracture surface was then etched with chloroform for 30 min at room temperature to dissolve the PBSA phase. The etched surface was kept in vacuum for 12 h before coating it with gold/palladium (50/50) alloy. The morphology was then examined using the JEOL model JSM-820 SEM apparatus operated at an accelerating voltage of 15 kV.

XRD experiments were conducted on a Siemens-500 diffractometer in the transmission mode. The beam was Cu K_α radiation ($\lambda = 0.154$ nm) operated at 40 kV and 40 mA. The basal spacing (d_{001}) of the C20A powder before and after intercalation, was estimated from the position of the (001) peak in the XRD pattern.

Dispersability of the intercalated silicate layers in the two phase polymer matrix was evaluated with a JEOL model JEM-1230 TEM, operated at an accelerating voltage of 80 kV. The TEM specimens were about 50–70 nm thick and were prepared by ultramicrotoming the nanocomposite samples encapsulated in an epoxy matrix with a diamond knife.

Dynamic mechanical properties of homopolymers, unmodified and organoclay-modified blends were measured by using a Rheometrics Scientific Analyzer (RSA) in the dual cantilever bending mode. The temperature dependence of storage flexural modulus (E') of homopolymer, virgin and C20A-modified blends was measured at a constant frequency (ω) of 6.28 $rad \cdot s^{-1}$ with a strain amplitude of 0.02% and in the temperature range of −65 to 70 °C with a heating rate of 2 $°C \cdot min^{-1}$. The linear viscoelastic zone was assessed by performing a series of strain sweep tests at a frequency of 6.28 $rad \cdot s^{-1}$.

Test specimens for the tensile measurements were prepared from 1.5 mm thick plates according to the ASTM D-638. Tensile modulus, tensile strength at yield, and elongation at break were measured in a tensile Instron 88215 tester (load 5 kN) with a cross head speed of 5 $mm \cdot min^{-1}$ at room temperature. The data presented here are averages of eight tests with a maximum error of 9%.

The thermogravimetric analysis (TGA) was conducted on a TGA Q500 TA Instrument at a heating rate of 10 $°C \cdot min^{-1}$ in air atmosphere, from room temperature to 600 °C.

Melt rheological measurements were performed on compression molded samples using a Paar-Physica Modular Compact Rheometer (MCR 501) at 190 °C in a nitrogen atmosphere to avoid any degradation of polymer matrices during measurements. Dynamic oscillatory shear measurements were performed by

applying a time dependent strain of:

$$\gamma(t) = \gamma_0 \sin(\omega t) \tag{2}$$

with the resultant shear stress being,

$$\sigma(t) = [G' \sin(\omega t) + G'' \cos(\omega t)] \tag{3}$$

with G' and G'' being the storage and loss modulus, respectively. Measurements were conducted by using a set of 25 mm diameter parallel plates with a sample thickness of 1–1.2 mm at 190 °C in a nitrogen environment. The strain amplitude was fixed to 5% to obtain reasonable signal intensities even at elevated temperature or low ω to avoid the nonlinear response. For each sample investigated, the limits of linear viscoelasticity were determined by performing strain sweeps at a series of fixed values of ω. Steady-shear viscosity measurements were conducted at 190 °C using 25 mm diameter cone and plate geometry with a cone angle of 0.1 rad.

Non-isothermal crystallization of various samples was performed on a TA DSC model Q100 series instrument under constant nitrogen flow. Samples were first heated to 200 °C at a heating rate of 30 °C · min^{-1}, held at that temperature for 5 min to eliminate any previous thermal history, and then cooled to 0 °C at constant cooling rate of 10 °C · min^{-1}. The organically modified blend samples were weighed such that all of the samples had identical polymer matrix content with respect to unmodified blend samples. The sample weight was maintained at low levels (4–5 mg) for all measurements in order to minimize any possible thermal lag during the scans. Each reported result was an average of four separate measurements. Temperature and heat of fusion were calibrated with an indium standard, and the base line was checked according to TA Instruments protocols.

Results and Discussion

Structure and Morphology of Homopolymer/C20A Hybrids

On the basis of Equation (1), one can describe thermodynamically that the compatibilization efficiency of a filler 'S' directly depends on the degree of its interaction with both polymer matrices. However, due to the intercalation chemistry, the compatibilization activity of clay is different from the common compatibilizer or other inorganic nanoparticles. Recently, Sinha Ray et al.[36] have demonstrated the true role of organically modified clay on immiscible PP/polystyrene (PS) blends. TEM images at high magnification revealed clear localization of intercalated silicate layers at the interface between the phases.

Now to determine the degree of interaction of C20A surface with each homopolymer matrix, 5 wt.-% of C20A was mixed with 95 wt.-% of PBSA, PPa, PPb, and PPc individually. Generally, the degree of interaction of clay surface with polymer matrix determined by the extent of intercalation of polymer chains into the two dimensional

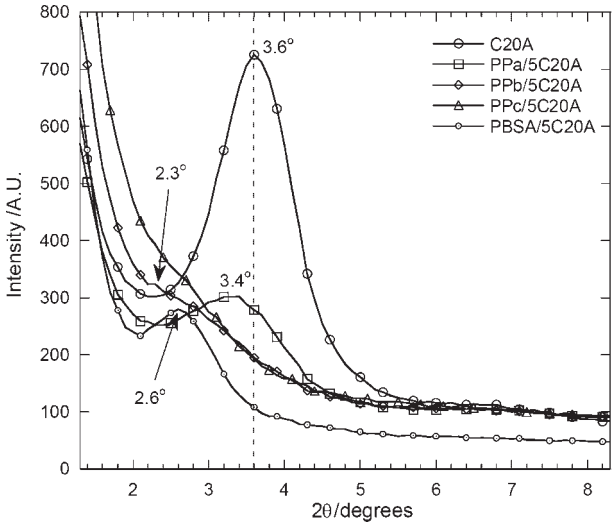

Figure 2. XRD patterns of pure C20A powder and various homopolymers based nanocomposites. The dashed line indicates the location of the silicate (001) reflection of pure C20A powder.

silicate galleries of clay. Direct evidence of the intercalation of the polymer chain into the silicate galleries is provided by XRD patterns in the range of $2\theta = 1$–10°. Figure 2 represents the XRD patterns of pure C20A powder and various homopolymer based composites.

The characteristic mean interlayer spacing of the (001) plane ($d_{(001)}$) for the C20A solid is 2.48 nm. In the case of PBSA/C20A hybrid, the intensity of the characteristic peak of C20A is significantly reduced due to the dilution effect and shifted to the smaller angle due to the intercalation of PBSA chains into the silicate galleries (see Figure 2). This corresponds to an interlamellar $d_{(001)}$-spacing of 3.68 nm. For the PPa/C20A hybrid such a distance is 2.58 nm. This result is obvious because the PPa matrix has a very low degree of interaction with C20A surfaces. In the XRD pattern of the PPb/C20A nanocomposite, the characteristic peak of C20A has almost disappeared with a small shoulder peak appearing at $2\theta = 2.3^\circ$, suggesting the formation of highly disordered intercalated nanocomposites. Finally, for the PPc/C20A hybrid, the characteristic peak of C20A has completely disappeared, indicating the formation of either exfoliated or highly disordered intercalated structure.

To support XRD results, TEM observations were used to directly and qualitatively visualize the state of silicate layer dispersion/exfoliation in various homopolymer matrices. Typical TEM bright field images of the nanocomposites are presented in Figure 3a–d. Figure 3a is a TEM bright filed image of PBSA/C20A nanocomposite. Stacked and intercalated silicate layers are clearly observed in the TEM image of the PBSA/C20A nanocomposite. Large agglomerates of the silicate layers are clearly seen in the case of the PPa/C20A hybrid, indicating very low level

Macromol. Mater. Eng. **2007**, *292*, 729–747

Macromolecular Journals

DOI: 10.1002/mame.200700029

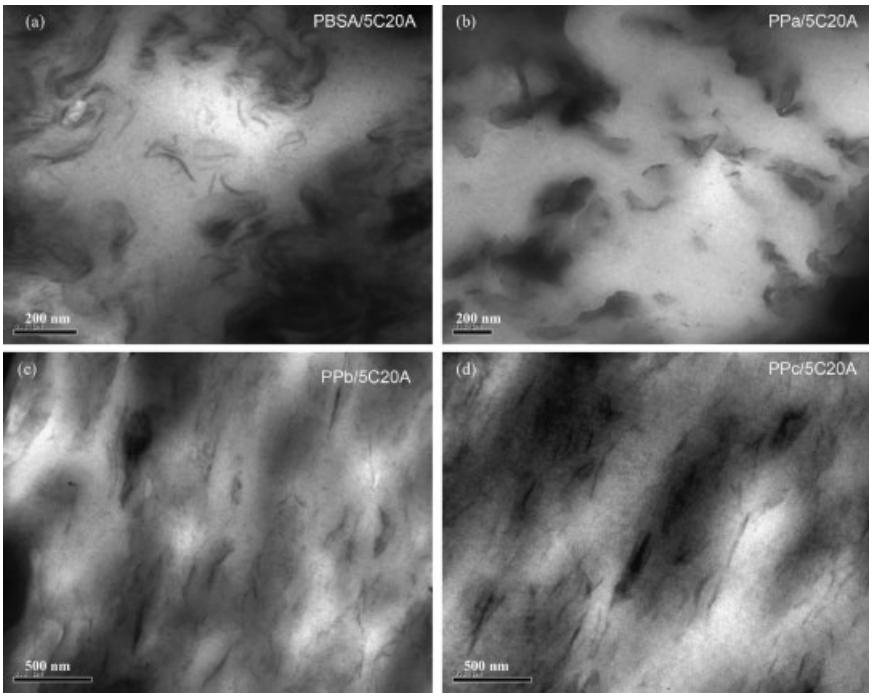

Figure 3. TEM bright field images: (a) PBSA/5C20A, (b) PPa/5C20A, (c) PPb/5C20A and (d) PPc/5C20A nanocomposites. The dark entities are the cross section of intercalated organoclay layers and the bright areas are the matrices.

of intercalation of PPa chains into the silicate galleries. This is consistent with the XRD pattern observed in the case of the PPa/C20A hybrid as shown in Figure 2. In the case of the PPb/C20A nanocomposite highly disorder intercalated silicate layers are dispersed in the PPb matrix. Although XRD patterns are featureless, few stacked and intercalated silicate layers are clearly observable in the PPc-based nanocomposite, Figure 3d. This indicates that intercalated silicate layers are disorderly oriented into the PPc-matrix.

On the basis of these XRD results and TEM observations, we can divide our blends into two categories. First, the PPa/PBSA blend where clay polymer interaction is more favorable in the case of PBSA than PPa and the intercalated silicate layers are therefore expected to be dispersed mainly in the PBSA phase. Secondly, in the PPb/PBSA or PPc/PBSA blends, both polymer matrices have some degree of favorable interactions with the clay surface, and hence no preferential dispersion of silicate layers is expected.

Morphology and XRD-Patterns of Various Blends

Taking into consideration the different degrees of interaction of C20A surfaces with PBSA, PPa, PPb, and PPc-matrices, the aim of this work is to find out whether C20A incorporation can change the morphology of PP/PBSA blends. Phase morphologies of various virgin and C20A modified PP/PBSA blends are presented in Figure 4, where a comparison is made from the chemically etched freeze-fractured surface of annealed (at 60 °C for 7 h under vacuum) compression-molded samples. The SEM typical morphology of the virgin PPa/PBSA blend shown in Figure 4a clearly demonstrates a two-phase morphology, where hollow domains indicate the extracted PBSA phase. This result indicates the expected immiscibility of the components. Micrograph Figure 4b represents the SEM image of a fracture surface of PPb/PBSA blend with the same weight ratio as in Figure 4a, but here PP is grafted with 0.2 wt.-% of MA. It is very interesting to note that the domain size of the dispersed PBSA matrix was significantly reduced in the presence of 0.2 wt.-% of MA as compare to that of the PPa/PBSA blend. The mixing of PBSA with PPc, containing 0.5 wt.-% of MA causes a further reduction in PBSA domain size, Figure 4c. Therefore, it is clear from the above results that the MA does play a role of compatibilizer in reducing the domain size of PBSA matrix in the PPb/PBSA and PPc/PBSA blends.

Figure 4a′ represents the morphology of the fractured surface of the PPa/PBSA blend with the same weight ratio as in Figure 4a but containing 5 wt.-% C20A. It is clear from the images that the blend morphology significantly changed after addition of C20A and leads to a typical oriented co-continuous morphology. While the addition of C20A either in PPb/PBSA or PPc/PBSA blends, the blends morphology shows significant reduction in domain size (see Figure 4b′ and c′) that means a high level of mixing between two polymer matrices.

Two possible explanations might be proposed regarding the transformation of domain-matrix structure to typical oriented co-continuous morphology in the case of the PPa/PBSA blend and the significant reduction in domain size in the case of the PPb/PBSA and PPc/PBSA blends: (i) dispersion of intercalated layers in both phases due to the common intercalation at the interphase, and (ii) clay platelets change the rheological properties of the blend. This second possibility will be discussed in a separate section.

To investigate the dispersion of intercalated silicate layers in the blend matrix, XRD analyses were carried out for the pure C20A and C20A-modified PP/PBSA blends. Figure 5a shows XRD patterns of the pure C20A powder and C20A-modified PPa/PBSA blend. For a better under-

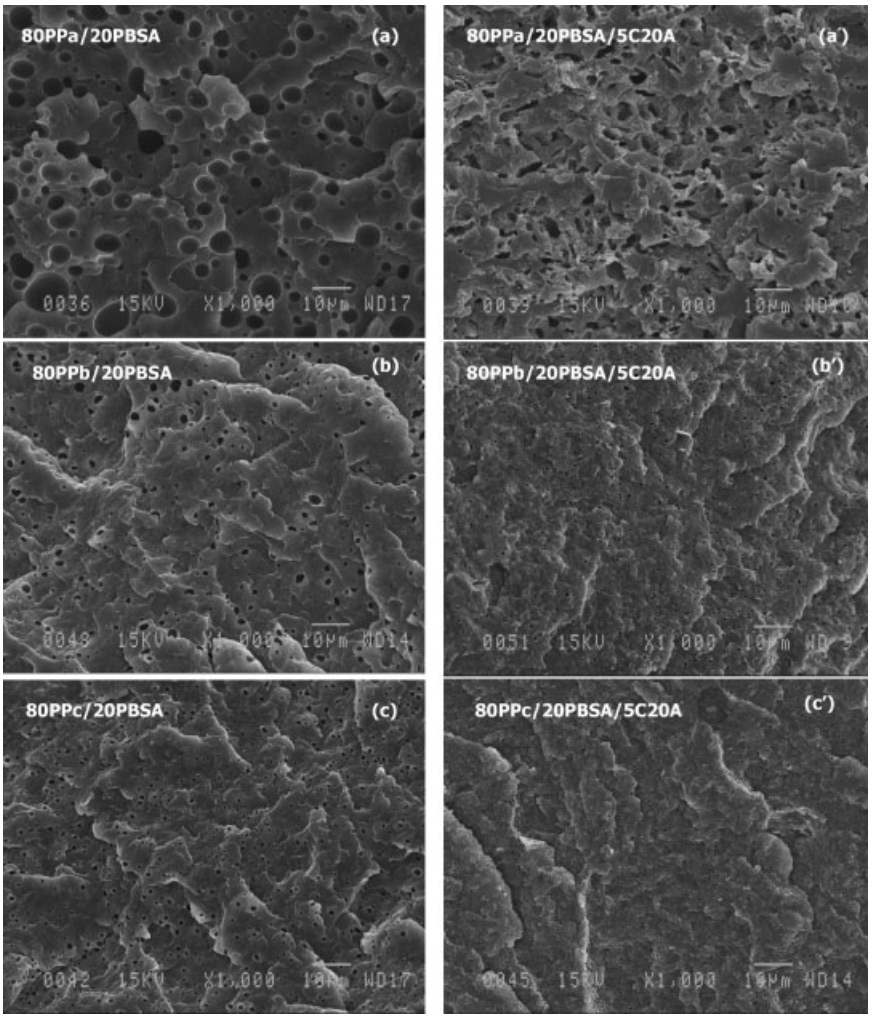

Figure 4. Phase morphologies of chemically etched freeze-fractured surface of annealed (at 60 °C for 7 h under vacuum) compression-molded samples of various virgin and C20A modified PP/PBSA blends.

standing, XRD patterns of hybrids of PBSA and PPa with 5 wt.-% of C20A are also described in the figure. For the PPa/C20A hybrid, the characteristic peak of C20A ($2\theta = 3.6^\circ$) shifts slightly to a lower angle ($2\theta = 3.42^\circ$), which indicates that very few PPa chains are intercalated into the silicate galleries. In the case of PBSA/C20A nanocomposite, the intensity of the characteristic peak of C20A is significantly reduced and shifts to a much lower angle ($2\theta = 2.62^\circ$) indicating the high degree of intercalation of PBSA chains into the silicate galleries. Finally, in the case of the PPa/PBSA/C20A blend, a sharp peak appears at $2\theta = 2.8^\circ$. It is very interesting to note that the intensity of the characteristic peak of C20A is increased in the case of the PPa/PBSA/C20A blend and the peak position is shifted to a lower angle than the PPa/C20A composite, but moves slightly to a higher angle than that of the PBSA/C20A nanocomposite. This observation indicates that both PBSA and PPa chains are intercalated into the same silicate galleries. During the melt-mixing process, C20A powder was slowly added into the blend. Since the PBSA matrix has a higher degree of interaction, most of the silicate layers are intercalated by the PBSA chains, but few galleries are intercalated by the PPa matrix. For this reason, in the case of the PPa/PBSA/C20A blend the XRD peak position significantly shifts to the lower angle with respect to the PPa/C20A hybrid. However, this peak position is very close to the PBSA/C20A nanocomposite.

The XRD patterns of pure C20A powder and C20A-modified PPb/PBSA blend are shown in Figure 5b. For a better understanding of the XRD patterns, the nanocomposites of PBSA and PPb are also included in the figure. In the XRD patterns of the PPb nanocomposite, the characteristic peak of C20A almost disappears with a small shoulder peak at $2\theta = 2.3^\circ$ suggesting the formation of highly disordered intercalated nanocomposites. However, a sharp intercalated peak appears at $2\theta = 2.7^\circ$ in the XRD pattern of the PPb/PBSA/C20A blend. This is again due to the intercalation of both polymer chains into the silicate layers and this peak is mainly coming from the PBSA intercalated silicate layers. We will conform this from TEM observations.

However, the most interesting XRD pattern is observed in the case of the PPc/PBSA/C20A blend (see Figure 5c), where a small shoulder peak appears at a much lower angle ($2\theta = 2.4^\circ$) than that of the PBSA/C20A nanocomposite. A possible explanation is that because of very strong compatibility, the PPc/PBSA blend behaves like a single matrix with a much higher average degree of affinity to the C20A surface than the PPa/PBSA or PPb/PBSA matrix. For this reason, the XRD peak position of the blend is gradually shifted to the lower angle from PPa, to PPb and finally, to PPc. This observation also suggests that both PBSA and PPc chains are intercalated into the same C20A silicate layers. Because of this common intercalation, the domain size of the dispersed phase is significantly reduced.

To gain more insight into the dispersion of intercalated and exfoliated silicate layers in the blend matrix, TEM analyses were carried out. Figure 6 is a bright field TEM image of the PPa/PBSA blend that gives a general view of

Macromol. Mater. Eng. **2007**, *292*, 729–747

Macromolecular Journals

DOI: 10.1002/mame.200700029

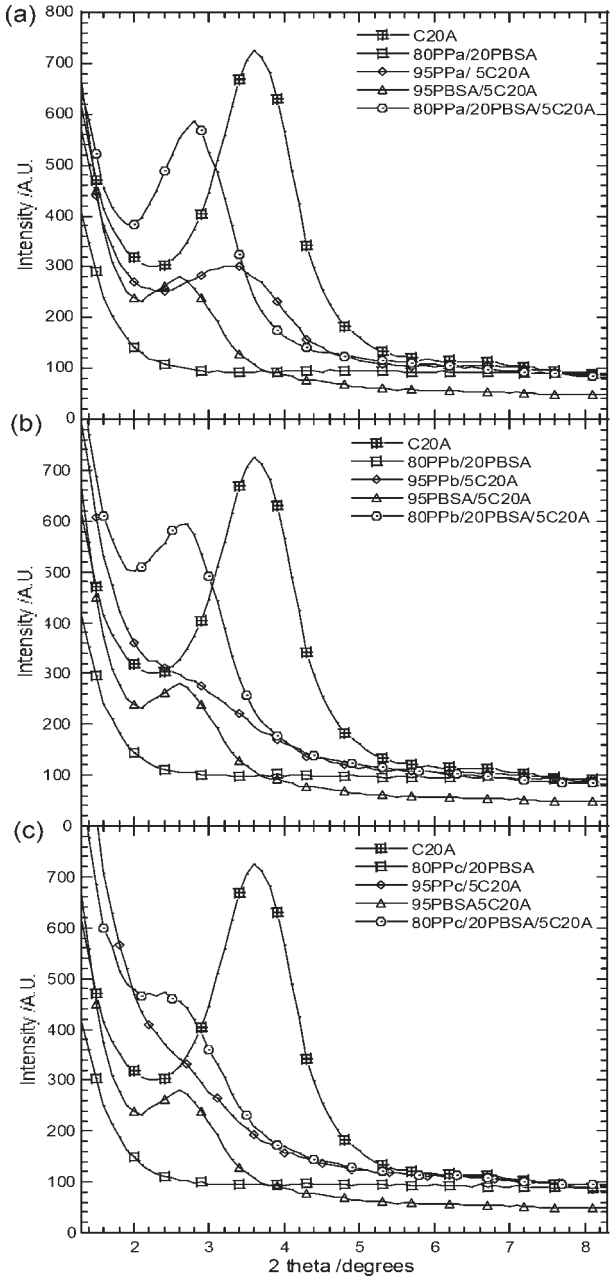

Figure 5. XRD patterns of unmodified and C20A modified blends: (a) 80PPa/20PBSA/5C20A, (b) 80PPb/20PBSA/5C20A, and (c) 80PPc/20PBSA/5C20A systems.

the dispersed PBSA domain in the PPa matrix. Figure 7a and b respectively represent the low and high magnification TEM images of the PPa/PBSA/C20A blend. The micrographs reveal that the highly stacked and intercalated silicate layers are dispersed in the blend matrix and it is very difficult to differentiate between two matrices. A possible explanation for this observation is that the PBSA matrix has a much higher degree of relative interactions with the C20A surface than the PPa matrix, but both

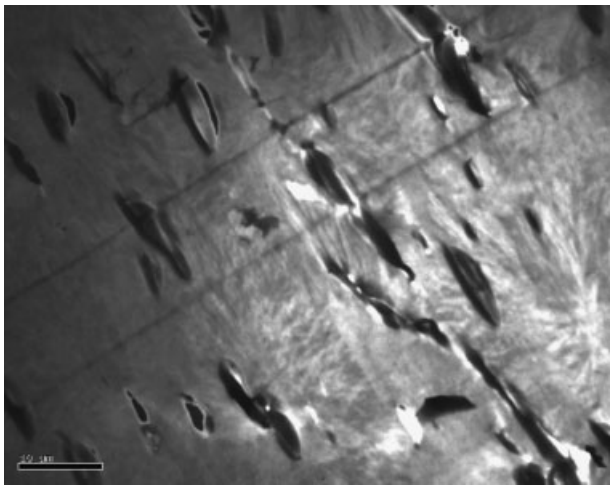

Figure 6. Bright field TEM image of 80PPa/20PBSA blend in which black ellipsoids correspond to the dispersed PBSA domains.

matrices are intercalated into the C20A silicate galleries, as can be seen in Figure 5a. In the XRD pattern of the PPa/PBSA/C20A blend, the characteristic peak appears in between the XRD peaks of PBSA/C20A and PPb/C20A nanocomposites but much closer to the PBSA/C20A nanocomposite peak. This indicates that C20A layers are mostly intercalated by the PBSA chains and few silicate layers are intercalated by the PPa polymer chains. For this reason the TEM image of the PPa/PBSA/C20A blend shows the presence of many stacked and intercalated silicate layers. These highly stacked and intercalated silicate layers are responsible for the sharp XRD peak. Because of this preferential dispersion of highly intercalated silicate layers, the viscosity of the PBSA matrix increases significantly and leads to the formation of typical oriented co-continuous structure. We will recall this explanation later.

Figure 7b and b′ represent the TEM images of the PPb/PBSA/C20A blend. The micrographs reveal the coexistence of disorder intercalated clay platelets and a majority of intercalated silicate layers are dispersed in the PPb/PBSA blend matrix. Highly disordered and relatively exfoliated along with very few stacked intercalated silicate layers are coexisting in the PPc/PBSA/C20A blend nanocomposite as can be seen in Figure 7c and c′. Only the stacked intercalated silicate layers are responsible for the weak XRD reflection, as is observed in Figure 5c, whereas the disordered or exfoliated silicate layers have no periodic stacking and thus remain XRD silent.[53,54] This type of relatively exfoliated structure with few stacked and intercalated silicate layers originates from the different degree of affinity of PBSA and PPc matrices to the C20A surface. Typically the PBSA intercalated silicate layers create stacked intercalated structure, whereas the PPc/

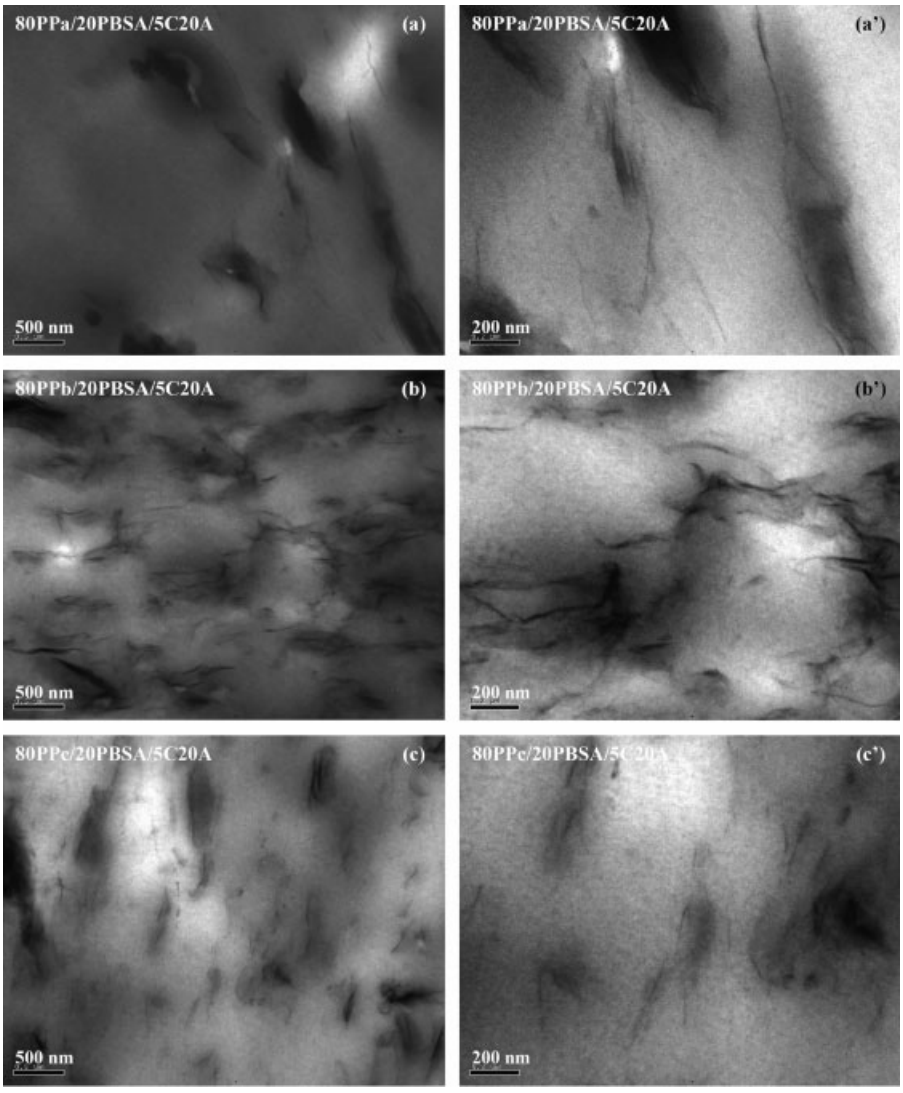

Figure 7. TEM bright field images of (a, a′) PPa/PBSA/C20A blend, (b, b′) PPb/PBSA/C20A blend, and (c, c′) PPc/PBSA/C20A blend.

C20A leads to the formation of exfoliated structure. The above observations suggest that the compatibility between the organically modified clay surface and the polymer matrix to a large extent, which plays a key role in the dispersion of the silicate layers within the blend matrix.

Dynamic Mechanical Analysis

Dynamic mechanical analysis (DMA) was used to measure the response of the virgin blend upon addition of organoclay to an oscillatory deformation in bending mode as a function of temperature.[55] Figure 8 represents temperature dependence of the storage modulus (E') of homopolymers, virgin and C20A-modified blends. Figure 8a shows the temperature dependence of E' of PBSA, PPa, PPa/PBSA and PPa/PBSA/C20A blends. At low temperature the PBSA matrix is in glassy state and it is characterized by an apparent glass transition (T_g) of about −42 °C that is revealed by a steep decrease in E' followed by a rubbery plateau. The modulus of the PPa matrix is much higher than that of the PBSA matrix and it is characterized by an apparent T_g of about −3 °C that is obtained by a sharp decrease in E' with temperature. In the case of the virgin PPa/PBSA blend, the value of E' decreases with respect to that of the PPa because of the highly phase separated morphology of the virgin blend. On the other hand, in the presence of the C20A platelets the modulus of the blend is significantly increased. A similar trend is observed in other blends (Figure 8b and c) with the same composition and they are prepared in a similar manner in a batch-mixer at 190 °C. However, the percentage of modulus improvement systematically varies from PPa/PBSA/C20A < PPb/PBSA/C20A < PPc/PBSA/C20A blends corresponding to their unmodified blends. These results are consistent with the dispersed domain sizes as presented in Figure 4. Therefore, these results clearly indicate that organoclay simultaneously acts as a compatibilizer and a nanofiller for immiscible polymer blends.

Tensile Properties

To further confirm the dual role of organoclay in the case of immiscible PP/PBSA blends, the mechanical properties of unmodified- and C20A-modied blends were measured in traction mode. The results are reported in Figure 9a–c for the tensile modulus, tensile strength at yield and elongation at break, respectively. The moduli of all blends without C20A are decreased with respect to that of corresponding PP matrices. Two reasons are responsible for the decrease in modulus: firstly, the formation of phase separated morphology that means it is not possible to

Macromol. Mater. Eng. **2007**, *292*, 729–747

DOI: 10.1002/mame.200700029

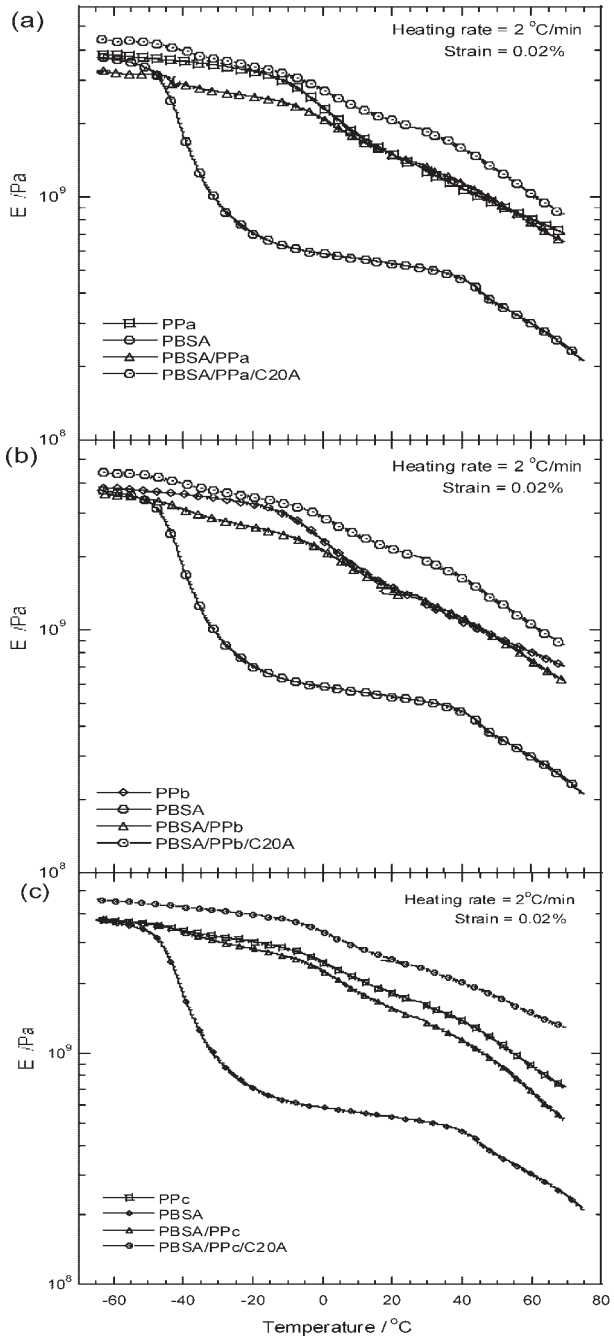

Figure 8. Temperature dependence of storage flexural modulus of various unmodified and C20A-modified PP/PBSA blends.

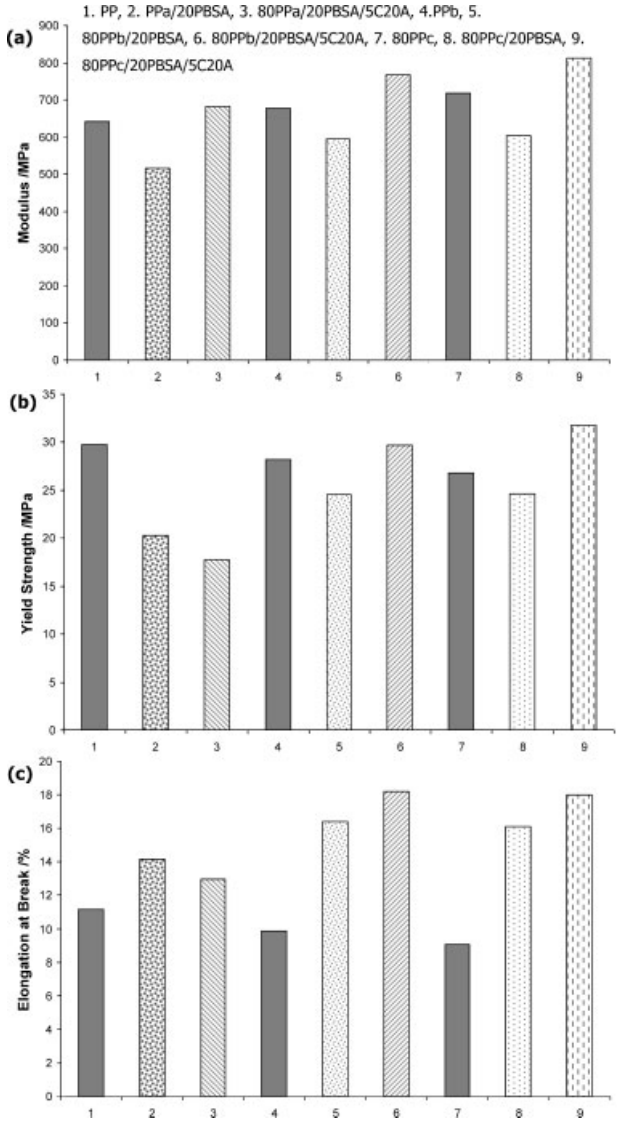

Figure 9. Tensile properties of various unmodified and C20A-modified PP/PBSA blends: (a) tensile modulus, (b) tensile strength at yield and (c) elongation at break.

transfer 100% stress between two polymer matrices, and, secondly, the very low value of modulus of PBSA matrix itself. The ≈200 MPa modulus value places PBSA in a very different category (not reported in Figure 9), something just beyond the stiff rubbers.[56] Therefore, it is very natural that addition of 20 wt.-% of PBSA matrix in PP matrices decreases the modulus of the blend. However, the addition of 5 wt.-% of C20A increases the modulus of blends. The biggest increase in modulus is observed upon the addition of C20A in the PPc/PBSA blend matrix. These results are consistent with the micrographs and XRD patterns as presented in Figure 4 and 5, respectively, which show the formation of typical co-continuous structure in the case of the PPa/PBSA/C20A blend and a high level of compatibilization in the case of the PPb/PBSA/C20A and PPc/PBSA/C20A blends, and the common intercalation of both polymer matrices in the same silicate layers.

The tensile yield strength of various virgin and C20A-modified blends is presented in Figure 9b. The tensile yield strength of all PP matrices decreases after incorporation of the PBSA matrix. Such a result is natural because of the phase separated morphology and the extent of decrease is

a maximum in the case of PPa/PBSA blend and a minimum in the case of the PPc/PBSA blend. Again, the addition of 5 wt.-% of C20A further decreases the tensile yield strength of the PPa/PBSA blend. However, in the case of PPb/PBSA and PPc/PBSA blends, the addition of C20A slightly increases the tensile yield strength with respect to the corresponding virgin blends. Clearly, in the last two cases the C20A platelets not only played the role of filler but also that of an interfacial active agent that promotes the maximum transfer of stress between two matrices.

Figure 9c represents the elongation at break of various unmodified- and C20A-modified blends. All virgin blends show significant improvement in elongation at break with respect to that of the corresponding PP matrices. Such an observation is very natural because PBSA matrix behaves like an impact modifier (very low modulus, ≈200 MPa). The elongation at break of the PPa/PBSA blend decreases after modification with 5 wt.-% of C20A, however, the elongation at break of the PPb/PBSA and PPc/PBSA blends further increases upon incorporation of C20A. This result indicates that C20A promotes the adhesion between PBSA and PPb or PPc matrices.

The above results fully confirm the dual role (nanofiller as well as compatibilizer) of organoclay in the case of immiscible polymer blends when both polymer matrices have some favorable interaction with organically modified clay surfaces.

Thermogravimetric Analysis

It has been established that the incorporation of layered silicate platelets into polymeric materials can improve their thermal stabilities.[57–59] In the case of polymer/clay nanocomposites, the increase in the thermal stability can be attributed to an ablative reassembling of the silicate layers which may occur on the surface of the nanocomposites creating a physical protective barrier on the surface of the material and, on the other hand, volatilization might also be delayed by the labyrinth effect of the silicate layers dispersed in the nanocomposites.[60] But in the case of polymer blend nanocomposites, the thermal stability also relates to the final morphology of the blend.[33]

The thermal stability of homopolymers, virgin and C20A-modified blends was measured by thermogravimetric analyzer (TGA) in air atmosphere. Sample weights were in the region of 11 ± 0.4 mg and placed into open platinum pans. Typically, three consecutive runs were conducted for each sample and averages are reported with an uncertainty of $\pm 1.56\,^{\circ}C$. Figure 10 shows the typical TGA traces of weight loss as a function of temperature of homopolymers measured in an air environment. It is clear from the figure that PBSA homopolymer shows much higher thermal stability than the PP matrices. This may be due to the higher crystallinity of PBSA matrix compared to that of PP matrices. Among PPa, PPb and PPc matrices, PPa shows higher thermal stability and PPb shows the least thermal stability, whereas the thermal stability of PPc is in between PPa and PPb matrices. At this moment it is not clear what mechanism causes the higher thermal stability of PPc.

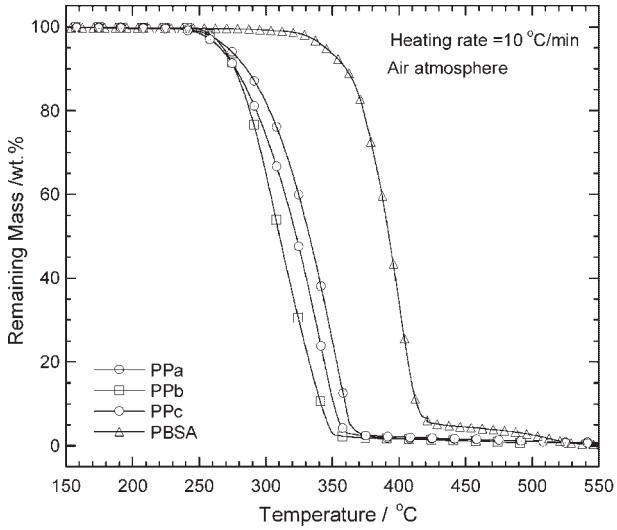

Figure 10. TGA thermograms of various homopolymers in air environment.

The TGA traces of virgin and C20A-modified blends are presented in Figure 11. The data available from TGA traces include: $T_{0.05}$, the temperature at which 5% degradation occurs, which is calculated from the intersection of the tangent of the initial point and considered as the onset temperature of degradation; $T_{0.5}$, the temperature at which 50% degradation occurs, which is another measure of thermal stability; and, finally, the non-volatile fraction at 500 °C, denoted as char formation. These data are summarized in Table 1.

Figure 11a represents the typical TGA traces of weight loss as a function of temperature of pure PPa, virgin and C20A-modified PPa/PBSA blends. It is clear from the figure that the thermal stability of PPa matrix significantly decrease after blending with PBSA matrix, although PBSA has much higher thermal stability than the PPa matrix. The unstable highly phase separated morphology (see Figure 4) is the main reason for reduced thermal stability of the virgin blend. Upon addition of 5 wt.-% of C20A, the thermal stability of the blend improves but is still lower than neat PPa matrix. Therefore, the co-continuous structure and stacked intercalated silicate layers does not lead to higher thermal stability of blend. Above 400 °C, slower degradation of PPa/PBSA/C20A blend is not surprising since there is only inorganic aluminosilicate left in the system at that stage.

Macromol. Mater. Eng. **2007**, *292*, 729–747

DOI: 10.1002/mame.200700029

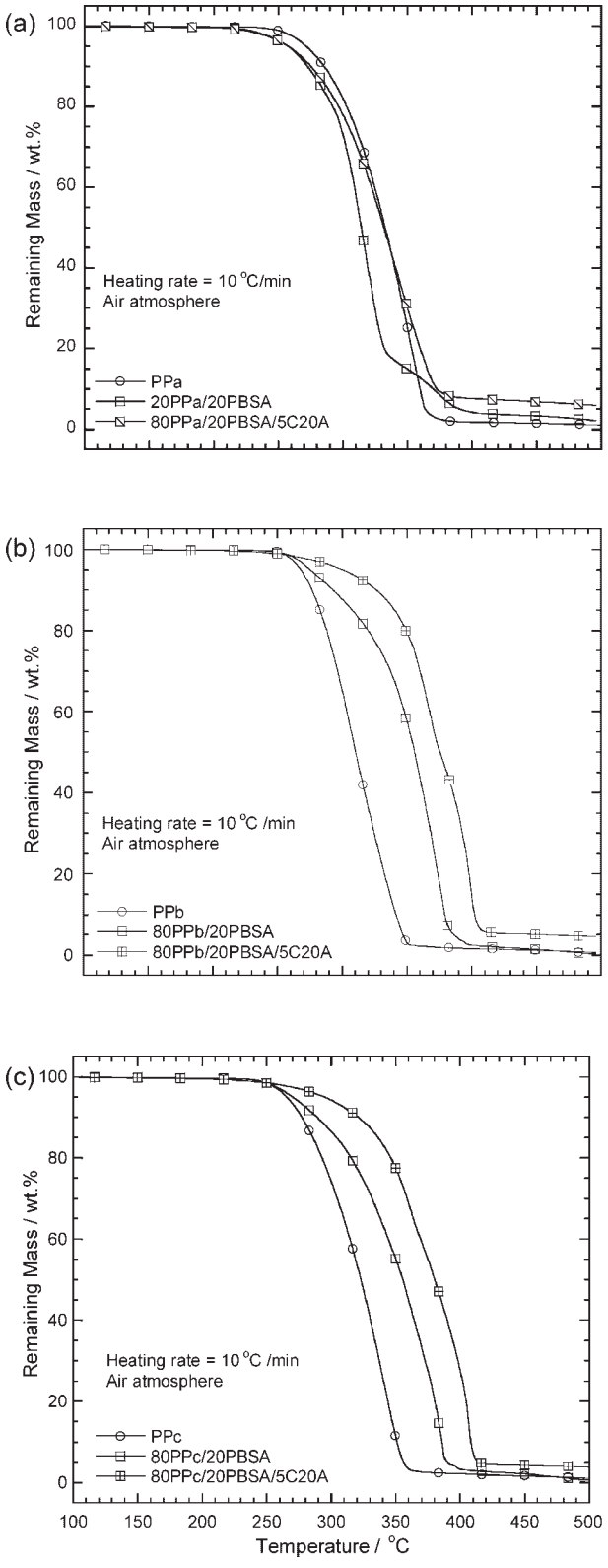

Figure 11. TGA thermograms of (a) virgin and C20A-modified PPa/PBSA blends, (b) virgin and C20A-modified PPb/PBSA blends and (c) virgin and C20A-modified PPc/PBSA blends in air.

Table 1. TGA data, in air atmosphere, for various homopolymers, virgin and C20A-modified PP/PBSA blends. Data are averages of three consecutive runs with an uncertainty of ±1.56 °C.

	$T_{0.05}$	$T_{0.5}$	Char at 500 °C
	°C	°C	%
PBSA	345.5	392.2	3.1
PPa	271.1	332.2	1.0
PPb	267.8	310.0	0.3
PPc	265.5	323.3	1.0
PPa/PBSA	254.5	314.5	2.1
PPa/PBSA/C20A	254.5	332.2	5.9
PPb/PBSA	275.5	355.6	0.3
PPb/PBSAC20A	300.0	375.6	4.5
PPc/PBSA	270.1	355.6	0.6
PPc/PBSA/C20A	294.5	380.1	3.8

On the other hand, the overall thermal stability of PPb/PBSA and PPc/PBSA blends dramatically improves as compared to those of corresponding PP matrices (Figure 11b and c). This is due to the high level of compatibility between PPb and PPc matrices with PBSA matrix as observed in Figure 4. The thermal stability of virgin blends further improves after modification with C20A. The very fine stable morphology of dispersed phase and the presence of homogeneously dispersed silicate layers in the blend matrices may be the main reason for the enhanced thermal stability of C20A-modified PPb/PBSA and PPc/PBSA blends. Again, because of a high level of compatibilization, the overall thermal stability of PPc/PBSA/C20A blend is higher than that of PPb/PBSA/C20A blend. These results are consistent with the final morphology of the blends as observed in Figure 4.

The first derivative TGA (dTGA) curves of various homopolymers and their unmodified and C20A-modified blends are shown in Figure 12. The dTGA curves are chosen for the presentation because they more clearly show the difference in thermal stability and exact degradation mechanism of all samples studied here. Figure 12a clearly shows that among PPa, PPa/PBSA, and PPa/PBSA/C20A samples, PPa has a higher thermal stability but PPa/PBSA/C20A has the lowest flammability.[60] However, it is very interesting to note that the PPa/PBSA sample shows a two step degradation, while both PPa and PPa/PBSA/C20A samples show only one step degradation. This result is consistent with the temperature dependent weight loss of PPa/PBSA sample, where a small deflection in curve is observed at around 330 °C. This behavior may be due the presence of highly phase separated morphology of PPa/PBSA blend. The lower temperature peak may be related

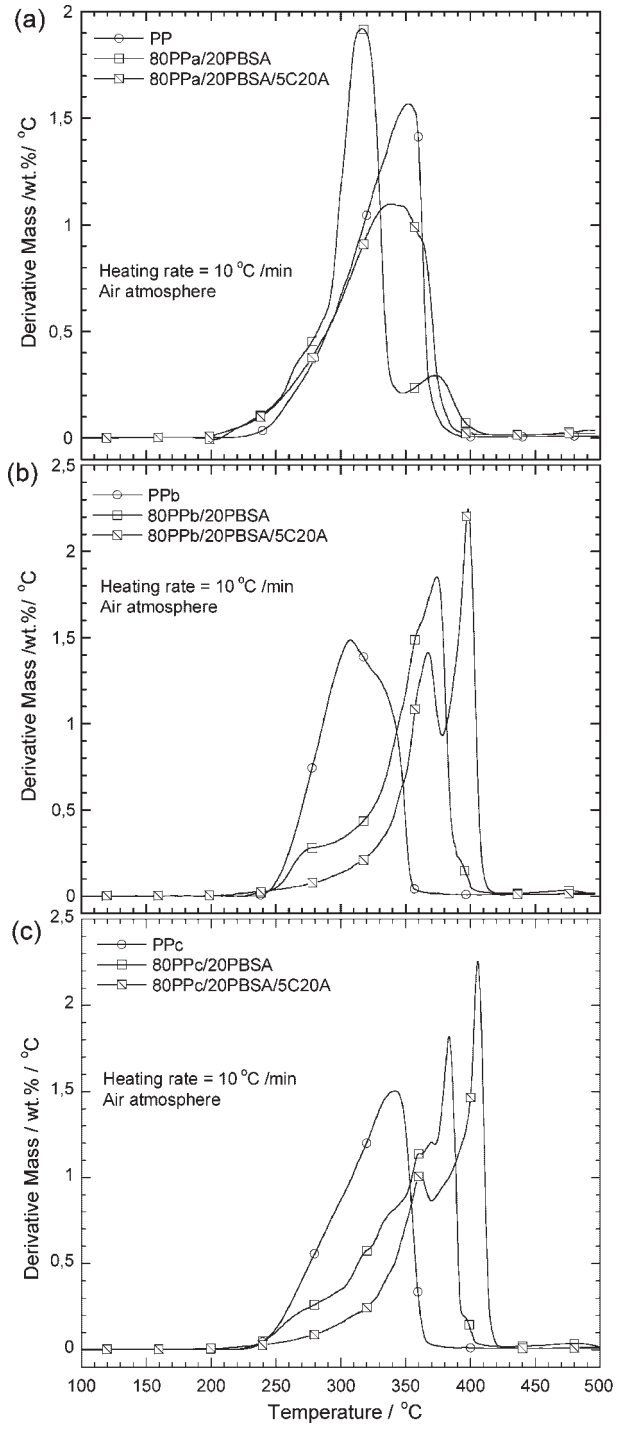

Figure 12. First derivative TGA (dTGA) curves of various virgin and C20A blends; (a) PPa/PBSA, (b) PPb/PBSA and (c) PPc/PBSA systems.

to the degradation of the PPa matrix and the higher peak temperature may be due to the PBSA matrix. However, the one step degradation of the PPa/PBSA/C20A sample may be due to the formation of typical co-continuous structure.

Like PPa/PBSA blends, two step degradation is also observed in the case of PPb/PBSA and PPc/PBSA blend samples and it is established from Figure 12b and c that the first step is related to the degradation of either PPb or PPc matrix, and the second step is related to the degradation of the PBSA matrix. However, in C20A-modified blends both peak temperatures shift to the much higher temperature range. This is due to the high level of intercalation of both polymer chains into the silicate galleries.

Melt Rheology

To examine the effect of the change in viscosity due to C20A addition, steady shear viscosity measurements were carried out for the virgin and C20A-modified blends. Here PPa/PBSA and PPb/PBSA blends are considered as model systems and rheological properties under molten state are

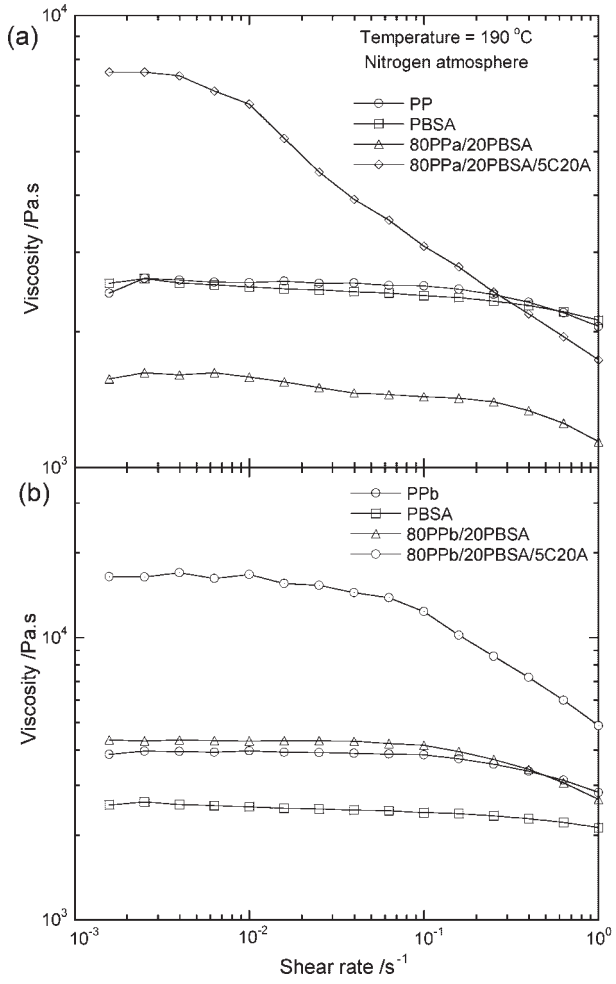

Figure 13. Shear rate dependence of viscosity of (a) PPa, PBSA, unmodified and C20A-modified PPa/PBSA blends and (b) PPb, PBSA, unmodified and C20A-modified PPb/PBSA systems measured at 190 °C in nitrogen.

Macromol. Mater. Eng. **2007**, *292*, 729–747

DOI: 10.1002/mame.200700029

described in detail. Figure 13a shows the change of steady shear viscosity of PBSA, PPa, virgin and C20A-modified PPa/PBSA blends measured at 190 °C in a nitrogen environment. The steady shear viscosity of virgin blend shows Newtonian behavior and the absolute value is lower than that of neat PBSA and PPa matrices. Such a result is obvious because of the highly phase separated morphology of the PPa/PBSA blend (see Figure 4). In the case of the PPb/PBSA blend, the viscosity of the virgin blend slightly increases compared to neat PPb. This is due to the much finer and stable morphology of the PPb/PBSA blend (see Figure 4).

The addition of C20A induces a strong viscosity for the PPa/PBSA blend at low shear rates; however, at high shear rates the viscosity value is still lower than that of virgin blend and pure polymer matrices. This behavior may be due to the slipping effect of C20A platelets for the highly phase separated PPa/PBSA system, where the PPa matrix has almost no interaction with C20A surface. On the other hand, C20A incorporation increases the viscosity of the PPb/PBSA blend significantly at all measured shear rates. This is due to the high level of mixing of both polymer matrices in the presence of C20A platelets and the homogeneous dispersion of highly intercalated silicate layers in the blend matrix.

It is generally accepted that the co-continuous morphology of a binary polymer blend can be formed within a composition region near the phase inversion.[37,61–67] The composition range is basically governed by the viscosity ratio of two components. To date, various equations have been used to predict the phase inversion composition.[61,64] According to Paul and Barlow,[61] the condition for phase inversion is expressed by:

$$\varphi_1\eta_2 = \varphi_2\eta_1 \quad (4)$$

where φ_i and η_i are the volume fraction and the melt viscosity of component *i*.

In order to investigate the mechanism of the morphological change of virgin PPa/PBSA blend in the presence of C20A, the viscosity corresponding to the conditions of mixing was measured. During the mixing process of the component in the batch mixer, the rotation speed was set at 60 rpm. This corresponds to an average shear rate of 50 s^{-1}.[68] The viscosity of PBSA, PPa and their nanocomposites with 5 wt.-% C20A at this shear rate was calculated on the basis of the equation described in ref.[68] and is reported in Table 2. The viscosity of pure PBSA and PPa matrices, and their nanocomposites with 5 wt.-% C20A was also measured in the dynamic mode. The results are shown in Figure 14. It is seen from Figure 13a and 14 and Table 2 that the viscosity of the PBSA matrix is almost comparable with the PPa matrix. With the addition of 5 wt.-% C20A in the PPa/PBSA blend system, the viscosity ratio of the two phases is slightly decreased to about 0.8 (from 0.9). It is also to be noted that a dramatic shear thinning behavior of PBSA/5C20A nanocomposite is observed in the dynamic oscillatory measurement but not in the case of PPa/5C20A nanocomposite (see Figure 14). This may be due to the selective localization of intercalated silicate layers in the PBSA matrix. Therefore, we believe that the viscosity ratio is not solely responsible for the dramatic change on PPa/PBSA phase morphology, but some other factors are also responsible which influence the phase morphology. At this moment it is very difficult for us to predict the exact mechanism for morphology change and details are under investigation.

Table 2. Viscosity of the PBSA, PPa, and C20A-based nanocomposites at a shear rate of 50 s^{-1}, calculated from batch mixer torque data.

Sample	Viscosity
	Pa · s
PBSA	804.5
95PBSA/5C20A	1 680.3
PPa	722.1
95PPa/5C20A	1 350.6

The angular frequency (ω) dependence of storage modulus, G' and loss modulus, G'' of neat PPa, PBSA, virgin and C20A-modified PPa/PBSA blend are presented in Figure 15a and b, respectively. At all frequencies, both G' and G'' for virgin PPa/PBSA blend decrease significantly

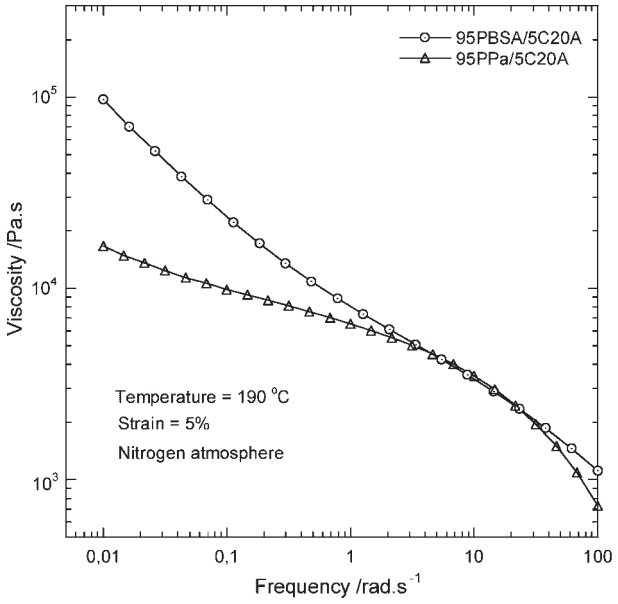

Figure 14. Dynamic complex viscosity of PPa/5C20A and PBSA/5C20A nanocomposites measured at 190 °C in a nitrogen atmosphere.

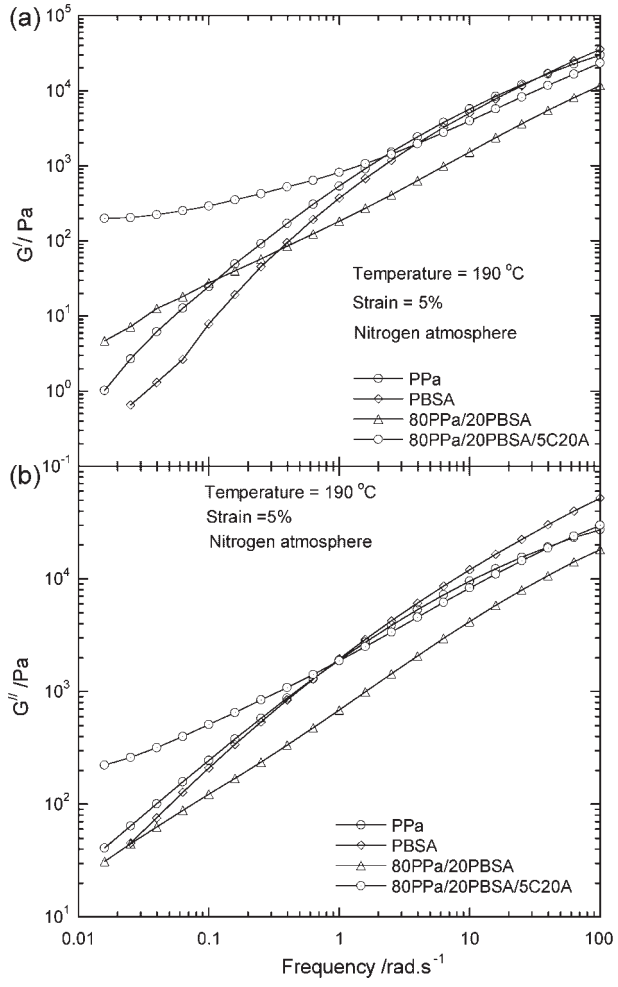

Figure 15. Reduced frequency dependence of the storage modulus, G' and the loss modulus, G'' of various unmodified and C20A-modified PPa/PBSA blends.

compared to those of the pure components. Such a result is due to the presence of highly dispersed PBSA phase in the PPa matrix. With the addition of 5 wt.-% of C20A in PPa/PBSA blend, at the high frequency region the viscoelastic response of the PPa/PBSA/C20A blend is almost identical to that observed for neat PPa. However, at the low-ω region, both dynamic moduli exhibit weak frequency dependence with C20A loading. This is due to the formation of co-continuous structure in the presence of C20A. According to this structure, the dispersed PBSA matrix and stacked-intercalated silicate layers are incapable of freely rotating[55] and hence the relaxation of the structure by imposing small frequency is partially prevented. This type of prevented relaxation is due to the highly geometric constraints of the co-continuous structure, which leads to the presence of the pseudo-solid-like behavior observed in the PPa/PBSA/C20A blend at low frequency regions. This behavior probably corresponds to the shear-thinning tendency, which strongly appears in the dynamic viscosity

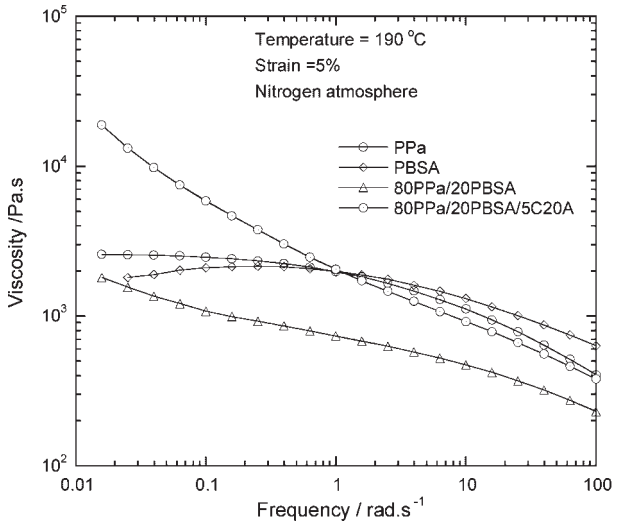

Figure 16. Dynamic complex viscosity of unmodified and C20A-modified PPa/PBSA blends measured at 190 °C in a nitrogen atmosphere.

curve of the PPa/PBSA/C20A blend (see Figure 16). The PPa/PBSA blend without clay also shows almost non-Newtonian behavior at all frequency ranges but the absolute value is lower than C20A-modified blend. This may be attributed to the presence of highly dispersed PBSA phase in the PPa matrix.

Figure 17a and b show the angular frequency dependence of G' and G'' of neat PPb, PBSA, unmodified- and C20A-modified PPb/PBSA blends. Unlike the PPa/PBSA system, the PPb/PBSA blend shows improvement in both G' and G'' with respect to that of the neat PPb at all frequencies. This is due to the high level of miscibility between PPb and PBSA matrices, which finally leads to the formation of a very fine stable morphology. Upon addition of 5 wt.-% of C20A, both moduli of PPb/PBSA further increase at all frequency ranges. In the high-ω region, the viscoelastic behavior of both unmodified- and C20A-modified blends is quite the same, with only a small increase in both moduli in the case of the C20A-modified blend, indicating that the observed chain relaxation modes are almost unaffected by the presence of the layered silicate particles. However, in the low-ω region both dynamic moduli exhibit weak frequency dependence in the case of the C20A-modified blend.

A reasonable explanation for this low-ω viscoelastic behavior of the PPb/PBSA/C20A blend is that the moderate interactions of both polymer matrices with C20A surface lead to the high degree of confinement of polymer chains inside the silicate layers. As a result, anisotropic silicate layers are fully dispersed in the PPb/PBSA matrix, as observed in XRD patterns and TEM images (Figure 4 and 5). Because of their highly anisotropic nature, disordered intercalated silicate layers form a network-type structure rendering the system highly elastic as revealed by the low

Macromol. Mater. Eng. **2007**, *292*, 729–747

Macromolecular Journals
DOI: 10.1002/mame.200700029

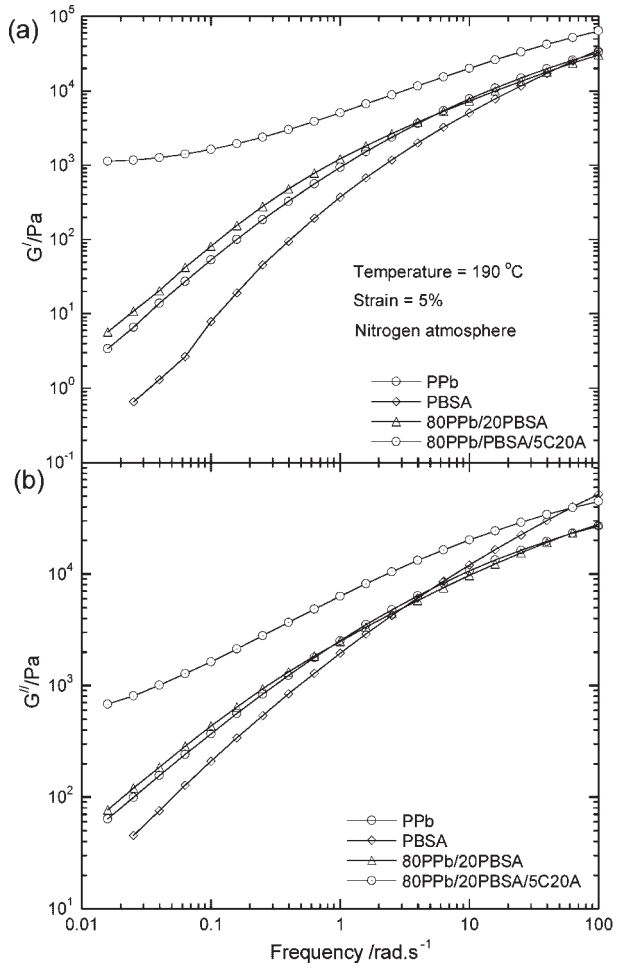

Figure 17. Reduced frequency dependence of the storage modulus, G' and the loss modulus, G'' of various unmodified and C20A-modified PPb/PBSA blends measured at 190 °C in a nitrogen atmosphere.

frequency plateau. Such a plateau is similar to that observed in rubber-toughened polymers,[69,70] where rubber particles form a percolating network that imparts the blend with solid-like behavior. Such a behavior can also be seen on the dynamic complex viscosity, shown in Figure 18. Little effect of C20A addition is observed at high frequencies, where the relaxation mechanism is mainly dominated by that of the blend matrix, whereas at low frequencies, the relaxation is that of particle-particle interactions inside the percolating network of the silicate layers.

Non-Isothermal and Cold Crystallization Behavior of Virgin and C20A-Modified Blends

In previous sections, mechanical and various other properties of virgin- and C20A-modified blends are described and it is found that the mechanical properties of virgin PP/

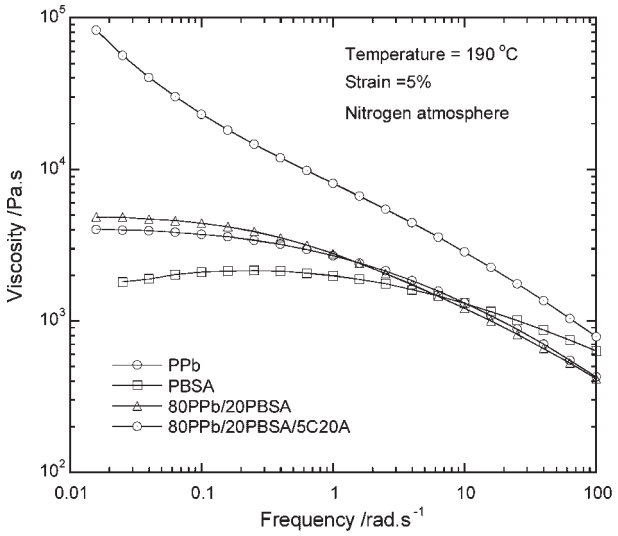

Figure 18. Dynamic complex viscosity of unmodified and C20A-modified PPb/PBSA blends measured at 190 °C in a nitrogen atmosphere.

PBSA blends concurrently improve in the presence of C20A when both polymer matrices have strong interactions with C20A surface. Now, in order to control the mechanical properties of the compatibilized blends during processing, it is essential to know the crystallization behavior of unmodified blend in detail and also how it is affected in the presence of clay particles. Usually researchers are interested in the polymer crystallization process under various isothermal conditions because the theoretical analyses are relatively easy and effects of the cooling rate and thermal gradients within the specimens can be easily excluded. However, the understanding of polymer crystallization behavior under dynamic conditions is of great importance, because most processing techniques actually occur under non-isothermal conditions. Moreover, non-isothermal crystallization can broaden and supplement the knowledge of the crystallization behavior of polymers. The main objective of this section is to report the effect of clay particles on the non-isothermal crystallization behavior of virgin PP/PBSA blend upon modification with C20A. Like the previous section, here we also choose PPa/PBSA and PPb/PBSA blends for our model systems because these blends show completely different morphology in the presence of C20A. In this section we will not discuss the non-isothermal crystallization kinetics of virgin and C20A-modified PP/PBSA blends because this is not the main theme of this study and we will report these findings separately.

To understand the non-isothermal crystallization behavior, all samples were first heated to 200 °C at a heating rate of 30 °C · min^{-1}, held at that temperature for 5 min to eliminate any previous thermal history, and then cooled to −10 °C at constant cooling rates of 10 °C · min^{-1}. The

crystallization exotherms of homopolymers, virgin, and C20A-modified blends for nonisothermal crystallization from the melt at 10 °C · min^{-1} are presented in Figure 19. The characteristic parameters of non-isothermal crystallization exotherms of neat PPa, PPb, PBSA and various unmodified and C20A-modified blends are summarized in Table 3.

It can be seen from Table 3 and Figure 19a that for the PPa sample with the addition of the PBSA matrix both crystallization onset (T_{on}) and crystallization peak (T_p) temperatures shift to the higher temperature region. The higher T_{on} and T_p of the PPa/PBSA blend matrix implies that the nucleating role of dispersed PBSA phase is active. With the incorporation of 5 wt.-% of C20A into PPa/PBSA blend, both T_{on} and T_p of the blend matrix further shifts to the higher temperature. This observation is quite common

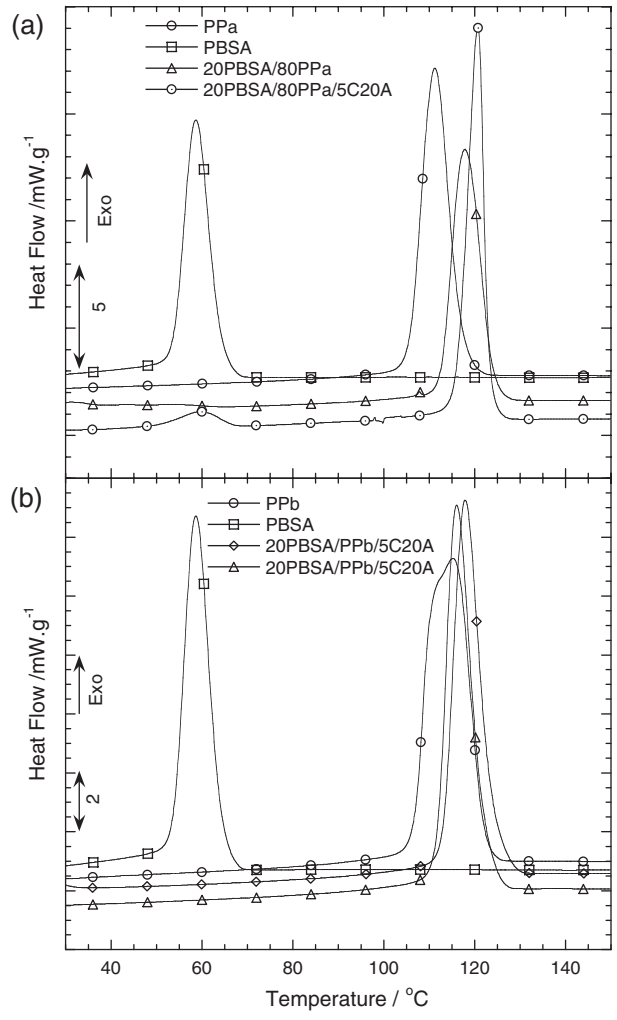

Figure 19. The crystallization exotherms of (a) neat PPa, PBSA, unmodified and C20A-modified PPa/PBSA blends and (b) neat PPb, PBSA, unmodified and C20A-modified PPb/PBSA blends for non-isothermal crystallization from the melt (at 200 °C) to 0 °C at a cooling rate of 10 °C · min^{-1}.

Table 3. The characteristic parameters of non-isothermal crystallization exotherms of neat PPa, PPb, PBSA, various unmodified and C20A-modified blends. Data are averages of three consecutive runs with an uncertainty of ±0.97 °C.

Sample	T_{on} [a]	T_{fin} [b]	T_p [c]	ΔH_{ex} [d]
	°C	°C	°C	J · g^{-1}
PBSA	78.7	22.0	58.6	60.8
PPa	132.9	86.9	111.0	119.9
PPa/PBSA	133.2	87.0	117.8	104.1
PPa/PBSA/C20A	133.9	90.8	120.7	102.5
PPb	136.8	91.7	115.0	118.4
PPb/PBSA	135.6	92.0	117.8	104.9
PPb/PBSA/C20A	135.4	91.5	116.2	98.28

[a] T_{on} is the crystallization onset temperature; [b] T_{fin} is the crystallization final temperature; [c] T_p is the crystallization peak temperature; [d] ΔH_{ex} is the crystallization enthalpy.

to the general understanding of the role of organoclay towards polymer crystallization.[71–75] But surprisingly, the total heat of crystallization (ΔH_{ex}) of the PPa matrix, estimated by integration of the area under the exothermic region of the DSC thermogram, decreases after blending with PBSA, which indicates that the degree of crystallinity of the PPa matrix is decreased. This may be due to the presence of dispersed PBSA domain in PPa matrix, which might hinder the local lameller crystallization and lead to the decrease in crystallinity of the PPa matrix. With the addition of C20A, the ΔH_{ex} value of the PPa/PBSA matrix further decreases. This is a result of intercalation of some PPa chains into the silicate galleries and the presence of PBSA chains intercalated silicate layers in the PPa matrix,[76] which further hinders the growth of PPa crystals.

On the other hand, in the case of the PPb/PBSA blend both T_{on} and T_p slightly move to the higher temperature range with respect to the PPb matrix. This indicates the nucleating ability of PBSA domains towards PP matrix crystallization is directly related to its size. However, in the presence of C20A, both T_{on} and T_p of PPb/PBSA blend are shifted to the lower temperature region. Not only that the ΔH_{ex} value of virgin blends significantly decreases in the presence of C20A platelets (see Table 3). We believe this is due to the high level of homogeneous dispersion of silicate layers in the blend matrix. This full dispersion of silicate layers in the blend matrix can be related to the favorable interaction of both polymer matrices with the C20A surface. The homogeneous dispersion of intercalated silicate particles in the blend matrix consequently acts as obstacles for mobility and flexibility of the polymer chains

Macromol. Mater. Eng. **2007**, *292*, 729–747

Macromolecular Journals

DOI: 10.1002/mame.200700029

to fold and join the crystallization growth front and lead to the decrease in value of ΔH_{ex}.

To determine the effect of C20A on the cold crystallization temperature of PPa/PBSA or PPb/PBSA blend samples, DSC scans of melt-quenched PPa, PPb, PBSA, and their virgin and C20A-modified blend samples were conducted. The sample are first annealed at 195 °C for 10 min inside a sealed aluminium pan to destroy any previous thermal history and subsequently quenched in liquid nitrogen. The samples were then transferred to the DSC cell, which had been previously set at −65 °C, as quickly as possible to measure the cold crystallization temperature of various samples at a heating rate of 20 °C · min^{-1}. Figure 20a and b show the DSC thermograms of various melt-quenched samples and various features are observed. The PPa matrix does not show any cold crystallization behavior at all. Like PPa, PPb also does not show any cold crystallization behavior but a small endothermic transition appears at about −19.5 °C; this may be a result of structural relaxation of PPb polymer chains during heating from the quenched state. On the other hand, a sharp crystallization exotherm appears at −13.7 °C for the PBSA sample. Only one prominent exotherm indicates that for the PBSA sample the cold crystallization process takes place from a single homogeneous phase.[76,77] For both PPa/PBSA and PPb/PBSA blend samples, this cold crystallization peak temperature moves to the higher temperature; this result may be due to the presence of the PP phase, which actually hinders the formation of PBSA crystals at low temperature.

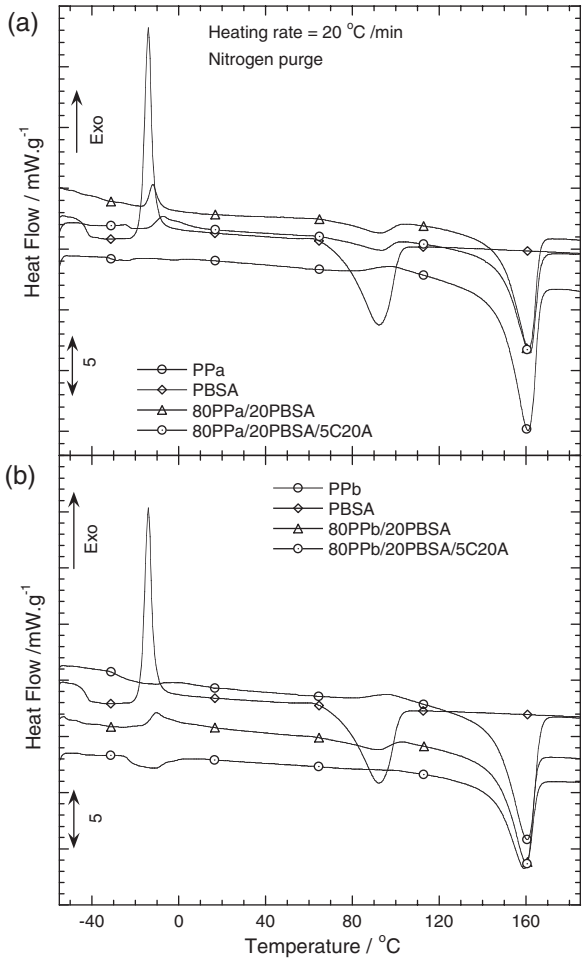

Figure 20. DSC thermograms of melt-quenched samples of (a) PPa, PBSA, unmodified and C20A-blends and (b) PPb, PBSA, unmodified and C20A-blends. The samples inside the aluminium pan were first annealed at 195 °C for 10 min to destroy any previous thermal history and subsequently quenched in liquid nitrogen. The samples were then transferred to the DSC cell, which was previous set at −65 °C, as quickly as possible.

In the case of the PPa/PBSA/C20A blend, very small exothermic, endothermic, and exothermic peaks appear, and the final exothermic peak corresponding to the cold crystallization of PBSA matrix appears at −7 °C. The appearance of first exothermic and then endothermic peaks may be due to the structural relaxation of PBSA chains during crystallization where PBSA chains are not fully relaxed before the crystallization. However, because of the selective intercalation of PBSA chains into the silicate galleries, the cold crystallization peak of PBSA is shifted to the higher temperature. On the other hand, in the case of the PPb/PBSA/C20A sample a broad endothermic peak appears at −15 °C. This may be a result of the structural relaxation of polymer chains during the heat scan. However, the absence of a PBSA cold crystallization peak in the case of the PPb/PBSA/C20A blend sample might be due to the common intercalation of both polymer chains into the silicate galleries.

Conclusion

In the present study, the effect of C20A platelets on the morphology and properties of two model systems such as PP/PBSA and PP-*g*-MA/PBSA blends has been investigated systematically. For the first polymer pair, the clay platelets are known to disperse in one phase, whereas for the second polymer pair, clay platelets are known to disperse in both components. The unmodified and C20A-modified blends are prepared by melt-mixing in a batch-mixer. The addition of C20A into the PP/PBSA blend changes the morphology from highly phase-separated to a typical co-continuous structure. This is attributed to the selective localization of intercalated silicate layers in the PBSA phase, which finally decreases the viscosity ratio of the blend matrices. On the other hand, the addition of C20A into PP-*g*-MA/PBSA blends reveals the efficient mixing of the polymer matrices. This is due to the common intercalation of both polymer chains into the same silicate galleries as revealed by XRD patterns and TEM observa-

tions. In all cases the extent of miscibility is directly reflected by significant improvements in the flexural bending modulus, tensile properties, and thermal stability. The melt-state rheological properties of virgin blends also improve in the presence of organoclay. All these results indicate that organoclay acts simultaneously as a nanofiller and as a compatibilizer when two chemically different polymers have strong interactions with organoclay surface.

DSC thermograms and subsequent calculations show that the incorporation of organoclay platelets in PP/PBSA blend matrix accelerates the mechanism of nucleation but decelerates the degree of crystallization of PP matrix. This is as a result of dispersion of the PBSA chains intercalated silicate layers in the PP matrix. On the other hand, the addition of organoclay particles in PP-*g*-MA/PBSA blend decelerates both the mechanism of nucleation and the crystal growth of PP-*g*-MA matrix. This is due to the full dispersion of silicate layers in the blend matrix, which subsequently act as obstacles for the mobility and flexibility of the PP-*g*-MA chains to fold and join the crystallization growth front, and hence lower the total heat of crystallization value. However, the homogeneous dispersion of intercalated silicate layers in PP-*g*-MA/PBSA blend matrix suppresses the cold crystallization exotherm of PBSA matrix.

Received: January 30, 2007; Revised: March 12, 2007; Accepted: March 12, 2007; DOI: 10.1002/mame.200700029

Keywords: blends; morphology; organoclay; poly(propylene)/poly[(butylene succinate)-*co*-adipate] blends; properties

[1] V. A. Fomin, V. V. Guzeev, *Prog. Rubb. Plastics. Tech.* **2001**, *17*, 186.
[2] S. Sinha Ray, M. Bousmina, *Prog. Mater. Sci.* **2005**, *50*, 962.
[3] J. Guillet, "*Encyclopedia of chemical technology*", Wiley-Interscience, New York 1984, p. 626.
[4] A. C. Albertsson, C. Barenstedt, S. Karlsson, T. Lindberg, *Polymer* **1995**, *36*, 3075.
[5] D. R. Ishioka, E. Kitakuni, Y. Ichikawa, "Aliphatic Polyesters: 'Bionolle'", in: *Biopolymers, Polyesters III. Application and Commercial Products*, Y. Doi, A. Steinbuchel, Eds., Wiley-VCH, Weinheim 2002, Vol. 4, p. 275.
[6] M. S. Nikolic, J. Djonlagic, *Polym. Degrad. Stab.* **2001**, *74*, 263.
[7] A. Ajji, "*Polymer Blends Handbook*", L. A. Utracki, Ed., Kluwer Academic, Dordrecht 2002 Chap. 4.
[8] S. B. Brown, "*Polymer Blends Handbook*", L. A. Utracki, Ed., Kluwer Academic, Dordrecht 2002 Chap. 5.
[9] J. M. Machado, C. S. Lee, *Polym. Eng. Sci.* **1994**, *34*, 59.
[10] T. K. Kwei, H. C. Frisch, W. Radigan, S. Vogel, *Macromolecules* **1977**, *10*, 157.
[11] C. E. Locke, D. R. Paul, *J. Appl. Polym. Sci.* **1973**, *17*, 2597.
[12] W. M. Barentsen, D. Heikens, P. Piet, *Polymer* **1974**, *15*, 119.
[13] R. Fayt, R. Jerome, Ph. Teyssie, *J. Polym. Sci. Part B: Polym. Phys.* **1981**, *19*, 1269.
[14] M. C. Schwarz, J. W. Barlow, D. R. Paul, *J. Appl. Polym. Sci.* **1988**, *35*, 2053.
[15] D. Hlavata, Z. Horak, J. Hromadkova, F. Lednicky, A. Pleska, *J. Polym. Sci. Part B: Polym. Phys.* **1999**, *37*, 1647.
[16] D. Hlavata, Z. Horak, F. Lednicky, J. Hromadkova, A. Pleska, Y. V. Zanevskii, *J. Polym. Sci. Part B: Polym. Phys.* **2001**, *39*, 931.
[17] G. Radonjic, V. Musil, I. Smit, *J. Appl. Polym. Sci.* **1998**, *69*, 2625.
[18] W. E. Baker, W. E. Saleem, *Polym. Eng. Sci.* **1987**, *27*, 1634.
[19] "*Encyclopaedic dictionary of commercial polymer blends*", L. A. Utracki, Ed., Chem.Tec. Publishing, Toronto 1994.
[20] H. Tanaka, A. J. Lavinger, D. D. Davis, *Phys. Rev. Lett.* **1994**, *72*, 2581.
[21] V. V. Ginzburg, F. Qiu, M. Paniconi, G. Peng, D. Jasnow, A. C. Balazs, *Phys. Rev. Lett.* **1999**, *42*, 4026.
[22] A. E. Nesterov, Y. S. Lipatov, *Polymer* **1999**, *40*, 1347.
[23] A. E. Nesterov, Y. S. Lipatov, T. D. Ignatova, *Eur. Polym. J.* **2001**, *37*, 281.
[24] Y. S. Lipatov, A. E. Nesterov, T. D. Ignatova, D. A. Nesterov, *Polymer* **2002**, *43*, 875.
[25] Y. S. Lipatov, *Prog. Polym. Sci.* **2002**, *27*, 1721.
[26] [26a] M. Alexandre, Ph. Dubois, *Mater. Sci. Eng.* **2000**, *R28*, 1; [26b] S. Sinha Ray, M. Okamoto, *Prog. Polym. Sci.* **2003**, *28*, 1539.
[27] S. Sinha Ray, M. Bousmina, A. Maazouz, *Polym. Eng. Sci.* **2006**, *46*, 1121.
[28] I. Gonzalez, J. I. Eguiazabal, J. Nazabal, *Euro. Polym. J.* **2006**, *42*, 2905.
[29] M. Si, T. Araki, H. Ade, A. L. D. Kilcoyne, R. Fisher, J. C. Sokolov, M. H. Rafailovich, *Macromolecules* **2006**, *39*, 4793.
[30] Y. Xu, W. J. Brittain, R. A. Vaia, G. Price, *Polymer* **2006**, *47*, 4564.
[31] M. H. Lee, C. H. Dan, J. H. Kim, J. Cha, S. Kim, Y. Hwang, C. H. Lee, *Polymer* **2006**, *47*, 4359.
[32] S. Sinha Ray, M. Bousmina, *Macromol. Rapid Commun.* **2005**, *26*, 450.
[33] S. Sinha Ray, M. Bousmina, *Macromol. Rapid Commun.* **2005**, *26*, 1639.
[34] Y. Li, H. Shimizu, *Macromol. Rapid Commun.* **2005**, *26*, 710.
[35] B. B. Khatua, D. J. Lee, H. Y. Kim, J. K. Kim, *Macromolecules* **2004**, *37*, 2454.
[36] S. Sinha Ray, S. Pouliot, M. Bousmina, L. A. Utracki, *Polymer* **2004**, *45*, 8403.
[37] Y. Li, H. Shimizu, *Polymer* **2004**, *45*, 7381.
[38] US 5091462 (1992), Ube Industries Ltd., invs.: O. Fukui, K. Tsutsui, T. Akagawa, I. Sakai, T. Nomura, T. Nishio, T. Yokoi, N. Kawamura; 1992.
[39] T. K. Chen, Y. I. Tien, K. H. Wei, *J. Polym. Sci. Part A: Polym. Chem.* **1999**, *37*, 2225.
[40] A. Tabtiang, S. Lumlong, R. A. Venables, *Polym. Plast. Technol. Eng.* **2000**, *39*, 293.
[41] US 6117932 Kabushiki Kaisha Toyota Chuo Kenkyusho, invs.: N. Hasegawa, H. Okamoto, M. Kawasumi, A. Usuki, A. Okada; 2000.
[42] S. M. Zhu, Y. Liu, M. Rafailovich, J. Sokolov, D. Gersappe, D. A. Winesett, H. Ade, *Abstr Pap ACS* **1999**, *218*, 109.
[43] V. Ferreiro, J. F. Douglas, E. J. Amis, A. Karim, *Macromol. Symp.* **2001**, *167*, 73.
[44] H. Wang, C. C. Zeng, M. Elkovitch, J. L. Lee, K. W. Koelling, *Polym. Eng. Sci.* **2001**, *41*, 2036.
[45] D. Voulgaris, D. Petridis, *Polymer* **2002**, *43*, 2213.
[46] M. Y. Gelfer, H. H. Song, L. Liu, B. S. Hsiao, B. Chu, M. Rafailovich, M. Si, V. Zaitsev, *J. Polym. Sci. Part B: Polym. Phys.* **2003**, *41*, 44.

DOI: 10.1002/mame.200700029

[47] Y. Wang, Q. Zhang, Q. Fu, *Macromol. Rapid Commun.* **2003**, *24*, 231.
[48] K. Yurekli, A. Karim, E. J. Amis, R. Krishnamoorti, *Macromolecules* **2003**, *36*, 7256.
[49] K. Yurekli, A. Karim, E. J. Amis, R. Krishnamoorti, *Macromolecules* **2004**, *37*, 507.
[50] S. Wang, Y. Hu, L. Song, J. Liu, Z. Chen, W. Fan, *J. Appl. Polym. Sci.* **2004**, *91*, 1457.
[51] S. Sinha Ray, unpublished results.
[52] Data sheet, Southern Clay Product Inc., Texas.
[53] S. Sinha Ray, K. Yamada, A. Ogami, M. Okamoto, K. Ueda, *Macromol. Rapid Commun.* **2002**, *23*, 943.
[54] S. Sinha Ray, K. Yamada, M. Okamoto, A. Ogami, K. Ueda, *Chem. Mater.* **2003**, *15*, 1456.
[55] S. Sinha Ray, M. Maiti, M. Okamoto, K. Yamada, K. Ueda, *Macromolecules* **2002**, *35*, 3104.
[56] S. Sinha Ray, M. Bousmina, M. Okamoto, *Macromol. Mater. Eng.* **2005**, *290*, 759.
[57] M. Zanetti, G. Camino, D. Canavese, A. B. Morgan, F. J. Lamelas, C. A. Wilkie, *Chem. Mater.* **2002**, *14*, 189.
[58] J. W. Gilman, C. L. Jackson, A. B. Morgan, P. Harris, *Chem. Mater.* **2000**, *12*, 1866.
[59] S. T. Lim, Y. H. Hyun, H. J. Choi, M. S. Jhon, *Chem. Mater.* **2002**, *14*, 1839.
[60] J. W. Gilman, T. Ksahiwagi, E. P. Giannelis, E. Manias, S. Lomakin, J. D. Lichtenhan, "*Fire retardancy of polymers*", M. Le Bras, G. Camino, S. Bourbigot, R. Delobel, Eds., The Royal Society of Chemistry, Cambridge 1998.
[61] D. R. Paul, J. W. Barlow, *J. Macromol. Sci. Rev. Macromol. Chem.* **1980**, *C18*, 109.
[62] G. M. Jordhamo, J. A. Manson, L. H. Sperling, *Polym. Eng. Sci.* **1986**, *26*, 507.
[63] I. S. Miles, A. Zurek, *Polym. Eng. Sci.* **1988**, *28*, 796.
[64] L. A. Utracki, *J. Rheol.* **1991**, *35*, 1615.
[65] B. D. Favis, J. P. Chalifoux, *Polymer* **1988**, *29*, 1761.
[66] R. M. Ho, C. H. Wu, A. C. Su, *Polym. Eng. Sci.* **1990**, *30*, 511.
[67] B. de Roover, J. Devaux, R. Legras, *J. Polym. Sci. Polym. Chem.* **1997**, *35*, 917.
[68] M. Bousmina, A. Ait-Kadi, J. B. Faisant, *J. Rheol.* **1999**, *43*, 415.
[69] M. Bousmina, R. Muller, *J. Rheol.* **1993**, *37*, 663.
[70] P. J. Carreau, M. Bousmina, A. Ajji, "*Rheological properties of blends. Facts and challenges in pacific polymers*", Springer Verlag, New York 1994.
[71] J. Y. Nam, S. Sinha Ray, M. Okamoto, *Macromolecules* **2003**, *36*, 7126.
[72] C. F. Ou, M. T. Ho, J. R. Lin, *J. Polym. Res.* **2003**, *10*, 127.
[73] Y. Ke, C. Long, Z. Qi, *J. Appl. Polym. Sci.* **1999**, *71*, 1139.
[74] N. Artzi, Y. Nir, D. Wang, N. Narkis, S. Siegmann, *Polym. Compos.* **2001**, *22*, 710.
[75] I. Y. Phang, K. P. Pramoda, T. Liu, C. He, *Polym. Int.* **2004**, *53*, 1282 and references cited therein.
[76] S. Sinha Ray, M. Bousmina, *Macromol. Chem. Phys.* **2006**, *207*, 1207.
[77] P. Xing, L. Dong, Y. An, Z. Feng, M. Avella, E. Martuscelli, *Macromolecules* **1997**, *30*, 2726.